J Sci Comput (2014) 61:61–89
DOI 10.1007/s10915-014-9818-0

Weighted Non-linear Compact Schemes for the Direct Numerical Simulation of Compressible, Turbulent Flows

Debojyoti Ghosh · James D. Baeder

Received: 29 July 2013 / Revised: 28 November 2013 / Accepted: 8 January 2014 /
Published online: 21 January 2014

Abstract A new class of compact-reconstruction weighted essentially non-oscillatory (CRWENO) schemes were introduced (Ghosh and Baeder in SIAM J Sci Comput 34(3): A1678–A1706, 2012) with high spectral resolution and essentially non-oscillatory behavior across discontinuities. The CRWENO schemes use solution-dependent weights to combine lower-order compact interpolation schemes and yield a high-order compact scheme for smooth solutions and a non-oscillatory compact scheme near discontinuities. The new schemes result in lower absolute errors, and improved resolution of discontinuities and smaller length scales, compared to the weighted essentially non-oscillatory (WENO) scheme of the same order of convergence. Several improvements to the smoothness-dependent weights, proposed in the literature in the context of the WENO schemes, address the drawbacks of the original formulation. This paper explores these improvements in the context of the CRWENO schemes and compares the different formulations of the non-linear weights for flow problems with small length scales as well as discontinuities. Simplified one- and two-dimensional inviscid flow problems are solved to demonstrate the numerical properties of the CRWENO schemes and its different formulations. Canonical turbulent flow problems—the decay of isotropic turbulence and the shock-turbulence interaction—are solved to assess the performance of the schemes for the direct numerical simulation of compressible, turbulent flows.

Keywords Direct numerical simulation · Compressible flows · Compact schemes · High resolution schemes · Compact schemes · CRWENO schemes

D. Ghosh (✉)
Applied Mathematics and Statistics, and Scientific Computation,
University of Maryland, College Park, MD 20742, USA
e-mail: ghosh@mcs.anl.gov

Present address:
D. Ghosh
Mathematics and Computer Science Division, Argonne National Laboratory, Lemont, IL 60439, USA

J. D. Baeder
Department of Aerospace Engineering, University of Maryland, College Park, MD 20742, USA
e-mail: baeder@umd.edu

1 Introduction

Compressible, turbulent flows are characterized by a large range of length scales as well as discontinuities such as shock waves. Numerical algorithms for such flows need to yield non-oscillatory solutions across discontinuities, as well as have a high spectral resolution to model all relevant length scales. The weighted essentially non-oscillatory (WENO) schemes [1,2] use a solution-dependent combination of lower-order interpolation schemes that is higher-order accurate for smooth solutions and non-oscillatory across discontinuities. The WENO schemes have been successfully applied to a large number of practical applications governed by hyperbolic conservation laws, including compressible flows [3]. Although WENO schemes of very high orders of accuracy have been implemented [4], one of their primary drawbacks in the context of turbulent flows is their low spectral resolution. Compact finite-difference schemes [5] have significantly higher spectral resolutions for the same order of convergence, as compared to non-compact finite-difference schemes. These schemes have been applied to the simulation of incompressible [6,7] and compressible [8,9] flows. The high spectral resolution of the compact schemes has resulted in their application to the direct numerical simulation (DNS) and large-eddy simulation (LES) of turbulent flows [10,11]. Linear compact schemes yield oscillatory solutions across discontinuities and a non-linearly stable compact scheme with a total variation bounded (TVB) limiter was introduced [12] for shock calculations and further improved [13].

Several high-resolution, non-oscillatory algorithms, proposed in the literature, combine the ENO and WENO schemes with compact schemes. One such family of algorithms are the hybrid schemes [14–16] where the local smoothness of the solution is used to switch between a compact scheme and the ENO or WENO scheme. A first-order detector is used to identify grid cells (along with a buffer region) where discontinuities are present. The ENO or WENO scheme is used to compute the flux derivatives at these cells and a compact scheme is used at all other cells. One of the primary drawbacks of these schemes is that they revert to a non-compact scheme with poor spectral resolution around discontinuities, resulting in a loss of accuracy for smaller length scales. This is more severe if the flow comprises a large number of discontinuities, e.g. shocklets, such that the hybrid algorithm would use the non-compact WENO scheme in the majority of the domain. Another family of algorithms that combines the compact schemes with ENO and WENO schemes are based on a non-conservative, staggered-mesh formulation for the flux derivative [17,18]. The two-stage reconstruction step uses the WENO scheme to interpolate the flux at the interfaces in a non-oscillatory manner and a central compact scheme is used to compute the derivative from the interface values. A similar ENO-Padé scheme, proposed in [19], achieved higher orders of accuracy at both stages of the reconstruction step. These schemes show only a marginal improvement of spectral resolution over the WENO schemes since they use a non-compact scheme to compute the interface fluxes.

A new class of non-linear compact schemes, proposed in [20], have a high spectral resolution and are non-oscillatory across discontinuities. The Compact-Reconstruction WENO (CRWENO) schemes are constructed by identifying lower order compact interpolation schemes at each interface and combining them using solution-dependent weights. The weights, based on the local smoothness of the solution, are identical to those used by the WENO schemes [2]. The resulting scheme is high-order accurate for smooth solutions and non-oscillatory across discontinuities. Fifth-order CRWENO schemes were constructed and their performance demonstrated on scalar conservation laws and the inviscid Euler equations [20,21]. The CRWENO schemes yield solutions with lower errors, compared to the WENO scheme of the same order of convergence. Significant improvements were observed in the

resolution of discontinuities and smaller length scales, as well as the preservation of flow features over large convection distances. The CRWENO schemes require the solution to a tridiagonal system of equations at each iteration. However, the additional expense is outweighed by the lower errors and the CRWENO schemes are computationally more efficient for scalar conservation laws and for the Euler equations when applied to the reconstruction of primitive or conserved variables. These schemes were applied to steady and unsteady flows around airfoils as well as wings and rotors [21,22], and several improvements were observed in the resolution of the boundary layer and wake flow features.

In addition to the numerical properties of the underlying linear schemes, the accuracy, convergence and resolution of the CRWENO (and the WENO) schemes depend on the implementation of the non-linear weights. The weights should attain their optimal values for smooth solutions such that the schemes converge to the underlying high-order accurate linear schemes. Across and near discontinuities, the weights corresponding to the lower-order schemes containing the discontinuity in its interpolation stencil should vanish, resulting in a non-oscillatory interpolation. The original formulation of the weights [2] had several drawbacks, including sensitivity to an arbitrary parameter (ϵ) as well as sub-optimal convergence for a class of smooth solutions [23]. In the context of turbulent flows, the non-linear weights are unable to distinguish between small length scales and discontinuities, thus introducing excessive numerical dissipation to the solution. Several attempts to improve the implementation of the non-linear weights have been presented in the literature in the context of the WENO schemes. These formulations alleviate some of these drawbacks and improve the accuracy and resolution of the WENO schemes. A mapping function was proposed [23] that accelerates the convergence of the weights to their optimal values, and reduces their sensitivity to an arbitrary parameter. However, the evaluation of the mapping function during the interpolation step adds significantly to the computational expense of the WENO algorithm. Alternative formulations for the weights have been suggested [24,25] that improve the behavior of the WENO schemes without the significant additional numerical cost.

This paper assesses and demonstrates the performance of the CRWENO schemes for the DNS of compressible, turbulent flows. The high spectral resolution of the underlying linear scheme (compact interpolation), compared to that of the WENO scheme (non-compact interpolation), indicates a more accurate modeling of the relevant length scales. In addition, the effect of the implementation of the non-linear weights is investigated in the context of the CRWENO schemes since further improvements are expected for intermediate and small length scales. The drawbacks of the CRWENO scheme implemented with the weights proposed in [2] are studied and the improved formulations for the weights are implemented. The schemes are applied to benchmark inviscid flow problems representative of compressible, turbulent flows, to assess their numerical properties. Finally, two canonical problems of turbulent flows—the decay of isotropic turbulence and the shock–turbulence interaction—are solved by applying the CRWENO scheme to the three-dimensional Navier–Stokes equations to demonstrate the performance of the CRWENO schemes for the DNS of turbulent flows. Section 2 reviews the fifth-order CRWENO scheme and the various implementations of the non-linear weights proposed in the literature for the WENO schemes. The numerical properties of the CRWENO schemes with the various non-linear weights are investigated through solutions to the linear advection equation as well as a non-linear spectral analysis in Sect. 3. Section 4 extends the CRWENO schemes to the Euler equations and demonstrates the numerical properties of the various formulations for illustrative inviscid flow problems. The numerical simulation of benchmark turbulent flow cases is presented in Sect. 5. Conclusions are drawn in Sect. 6.

2 CRWENO Schemes

The conservative, finite difference discretization of the spatial derivatives in a hyperbolic partial differential equation (PDE) requires the reconstruction of the interface flux $\hat{f}_{j+1/2}$ from its cell-centered values $f_j = f(u(x_j))$, where u is the conserved variable and $f(u)$ is the flux function. Solutions to hyperbolic PDEs comprise left- and right-running waves, and an upwind-biased interpolation is used to model the underlying physics of wave propagation. The CRWENO scheme is described in this section for a left-biased interpolation and the corresponding expressions for a right-biased interpolation can be trivially obtained. The general form of a compact interpolation scheme for the interface flux $\hat{f}_{j+1/2}$ is

$$A\left(\hat{f}_{j+1/2-m}, \ldots, \hat{f}_{j+1/2}, \ldots, \hat{f}_{j+1/2+m}\right) = B\left(f_{j-n}, \ldots, f_j, \ldots, f_{j+n}\right) \tag{1}$$

where the stencil operators A and B denote a linear combination of the terms inside the parentheses, and the indices m and n are the width of the stencils ($m > 0$ results in a system of equations while $m = 0$ corresponds to non-compact interpolation schemes). CRWENO schemes are constructed by identifying r candidate compact interpolation schemes of r-th order accuracy at each interface:

$$A_k^r\left(\hat{f}_{j+1/2-m}, \ldots, \hat{f}_{j+1/2+m}\right) = B_k^r\left(f_{j-n}, \ldots, f_{j+n}\right);\ k = 1, \ldots, r,\ m > 0 \tag{2}$$

where the superscript denotes the order of accuracy. There exist optimal coefficients $c_k;\ k = 1, \ldots, r$ such that the weighted sum is a $(2r-1)$-th order accurate compact interpolation scheme. This can be expressed as:

$$\begin{aligned} &\sum_{k=1}^{r} c_k A_k^r\left(\hat{f}_{j+1/2-m}, \ldots, \hat{f}_{j+1/2+m}\right) = \sum_{k=1}^{r} c_k B_k^r\left(f_{j-n}, \ldots, f_{j+n}\right) \\ &\quad \Rightarrow A^{2r-1}\left(\hat{f}_{j+1/2-m}, \ldots, \hat{f}_{j+1/2+m}\right) = B^{2r-1}\left(f_{j-n}, \ldots, f_{j+n}\right). \end{aligned} \tag{3}$$

The optimal weights are replaced by non-linear, solution-dependent weights, ω_k, that depend on the smoothness of the solution in the corresponding candidate stencil. The final CRWENO scheme can thus be expressed as:

$$\sum_{k=1}^{r} \omega_k A_k^r\left(\hat{f}_{j+1/2-m}, \ldots, \hat{f}_{j+1/2+m}\right) = \sum_{k=1}^{r} \omega_k B_k^r\left(f_{j-n}, \ldots, f_{j+n}\right). \tag{4}$$

This results in a system of equations with solution-dependent coefficients, unlike linear compact schemes. The solution to this system is required every iteration and cannot be computed as a pre-processing step.

Fifth-order accurate CRWENO schemes were constructed in [20,21]. A fifth-order CRWENO scheme can be constructed by combining three third-order compact schemes,

$$\frac{2}{3}\hat{f}_{j-1/2} + \frac{1}{3}\hat{f}_{j+1/2} = \frac{1}{6}\left(f_{j-1} + 5f_j\right); \quad c_1 = \frac{2}{10}, \tag{5}$$

$$\frac{1}{3}\hat{f}_{j-1/2} + \frac{2}{3}\hat{f}_{j+1/2} = \frac{1}{6}\left(5f_j + f_{j+1}\right); \quad c_2 = \frac{5}{10}, \tag{6}$$

$$\frac{2}{3}\hat{f}_{j+1/2} + \frac{1}{3}\hat{f}_{j+3/2} = \frac{1}{6}\left(f_j + 5f_{j+1}\right); \quad c_3 = \frac{3}{10}, \tag{7}$$

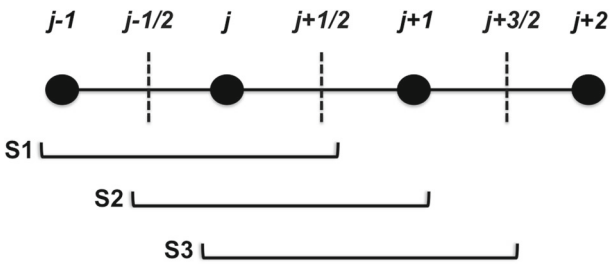

Fig. 1 Constituent compact stencils for the fifth-order CRWENO scheme: S1—(5), S2—(6), S3—(7)

where c_1, c_2 and c_3 are the corresponding optimal weights and the stencils are shown in Fig. 1. These yield an optimal fifth-order compact scheme,

$$\frac{3}{10}\hat{f}_{j-1/2} + \frac{6}{10}\hat{f}_{j+1/2} + \frac{1}{10}\hat{f}_{j+3/2} = \frac{1}{30}f_{j-1} + \frac{19}{30}f_j + \frac{1}{3}f_{j+1}. \tag{8}$$

Replacing the optimal weights with the non-linear weights results in the fifth-order CRWENO (CRWENO5) scheme,

$$\begin{aligned}\left(\frac{2}{3}\omega_1 + \frac{1}{3}\omega_2\right)\hat{f}_{j-1/2} + \left[\frac{1}{3}\omega_1 + \frac{2}{3}(\omega_2 + \omega_3)\right]\hat{f}_{j+1/2} + \frac{1}{3}\omega_3\hat{f}_{j+3/2} \\ = \frac{\omega_1}{6}f_{j-1} + \frac{5(\omega_1 + \omega_2) + \omega_3}{6}f_j + \frac{\omega_2 + 5\omega_3}{6}f_{j+1}.\end{aligned} \tag{9}$$

This interpolated flux is obtained by solving this tridiagonal system of equations. The scheme is fifth order accurate for smooth solutions. Across discontinuities, the weights corresponding to the stencils that contain the discontinuities go to zero. This results in a decoupling of the tridiagonal system [21, Sec. 2.2] and spurious oscillations are thus avoided.

The spatially discretized PDE results in an ordinary differential equation in time, which is solved using the third-order total variation-diminishing Runge-Kutta scheme (TVD-RK3) [28] in this paper.

2.1 Implementation of Non-linear Weights

The present implementation of the CRWENO5 scheme utilizes the non-linear weights formulated for the fifth-order WENO scheme that are functions of the local solution smoothness. The original formulation of the non-linear weights for the WENO schemes [2] defined them as

$$\alpha_k = \frac{c_k}{(\epsilon + \beta_k)^p} \tag{10}$$

$$\omega_k = \frac{\alpha_k}{\sum_k \alpha_k} \tag{11}$$

with $\epsilon = 10^{-6}$ and $p = 2$. The smoothness indicators are given by

$$\beta_1 = \frac{13}{12}\left(f_{j-2} - 2f_{j-1} + f_j\right)^2 + \frac{1}{4}\left(f_{j-2} - 4f_{j-1} + 3f_j\right)^2, \tag{12}$$

$$\beta_2 = \frac{13}{12}\left(f_{j-1} - 2f_j + f_{j+1}\right)^2 + \frac{1}{4}\left(f_{j-1} - f_{j+1}\right)^2, \tag{13}$$

$$\beta_3 = \frac{13}{12}\left(f_j - 2f_{j+1} + f_{j+2}\right)^2 + \frac{1}{4}\left(3f_j - 4f_{j+1} + f_{j+2}\right)^2. \tag{14}$$

The fifth-order CRWENO and WENO schemes with the non-linear weights given by (10) and (11) is referred to as CRWENO5-JS and WENO5-JS respectively for the remainder of this paper. Thus, the WENO5-JS scheme corresponds to the method proposed in [2]. Although there is an inconsistency between the stencils used for the smoothness indicators and those used for the CRWENO interpolation (Fig. 1), numerical results [20] indicate that this choice results in a high-order accurate, non-oscillatory scheme. Several linear and non-linear examples show that the CRWENO schemes retain the high-order accuracy for smooth solutions and non-oscillatory behavior across discontinuities. Formulating the smoothness-indicators based on a compact approximation to the derivatives at the given interface results in a non-linear system of equations for the interface flux and this approach is not pursued.

The parameter ϵ in (10) was introduced by [2] to prevent division by zero. However, it was demonstrated [23] that the convergence properties of the WENO5 scheme are sensitive to the value of ϵ for smooth solutions with vanishing derivatives. The mapped weights were introduced [23],

$$\alpha_k^M = g_k(\omega_k), \quad g_k(\omega) = \frac{\omega\left(c_k + c_k^2 - 3c_k\omega + \omega^2\right)}{c_k^2 + \omega\left(1 - 2c_k\right)}, \tag{15}$$

that improved the convergence of the non-linear weights to their optimal values. The CRWENO5 and WENO5 schemes with the mapped weights are referred to as CRWENO5-M and WENO5-M respectively in this paper.

In the context of the numerical simulation of flows with a large range of length scales, the WENO schemes [2] have two major drawbacks: the limited spectral resolution of the underlying linear scheme, and the dissipation introduced by the non-linear weights. The CRWENO scheme addresses the first of these drawbacks by using compact interpolations with significantly higher spectral resolution; however, further improvements are expected from the proper formulation of the non-linear weights. The weights, as formulated in [2], are not able to distinguish between discontinuities and small-length-scale waves; as a result, the smaller length scales in the solution are not captured accurately. The mapped weights alleviate this problem by improving the convergence of the weights to their optimal values, without compromising the non-oscillatory nature of the scheme. Thus, the numerical results in [23] show sharper resolution of discontinuities. The primary drawback of the mapping function is the additional computational expense required to calculate the mapped weights. Another drawback is that the mapped WENO scheme does not improve upon the original definition of the weights by mathematically distinguishing between discontinuities and smooth, small-length-scale waves.

Alternative implementations for the non-linear weights were proposed in [24,25], where the weights are defined as

$$\omega_k = c_k\left[1 + \left(\frac{\tau}{\beta_k + \epsilon}\right)^p\right]. \tag{16}$$

The factor τ is defined in [24] as

$$\tau = |\beta_1 - \beta_3|, \tag{17}$$

whereas it is defined in [25] as

$$\tau = \left(f_{j-2} - 4f_{j-1} + 6f_j - 4f_{j+1} + f_{j+2}\right)^2. \tag{18}$$

The CRWENO5 schemes using these weights are referred to as CRWENO5-Z and CRWENO5-YC, respectively (and similarly, WENO5-Z and WENO5-YC refer to the

Table 1 Implementation of non-linear weights for the CRWENO5 scheme

Name of Scheme	Implementation of weights	Author(s)
CRWENO5-JS	(10)	Jiang and Shu [2]
CRWENO5-M	(10), (15)	Henrick et al. [23]
CRWENO5-Z	(16), (17)	Borges et al. [24]
CRWENO5-YC	(16), (18)	Yamaleev and Carpenter [25]

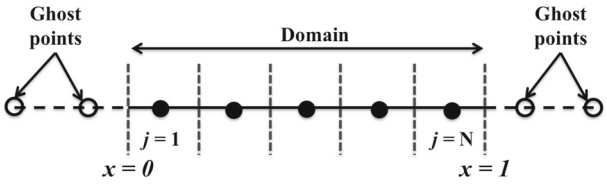

Fig. 2 Boundary closure implementation using ghost points

WENO5 schemes with these weights). Table 1 summarizes the implementations of the CRWENO5 scheme studied in this paper. In addition, some examples are presented in subsequent sections that compare the numerical properties of the CRWENO5 scheme with the WENO5 scheme. These schemes are referred to as "CRWENO5" and "WENO5" in the text and use the original formulation for the weights, as given by (10).

2.2 Boundary Closure

The implementation of the CRWENO scheme on a finite domain requires a boundary closure. In the present implementation, the domain is extended using ghost points, as shown in Fig. 2 for a one-dimensional domain of unit length and a grid with N interior points. The fifth-order WENO scheme (WENO5) [2] is used for the first and last interfaces. Assuming optimal weights, this can be expressed as:

$$j = 0:$$

$$\hat{f}_{1/2} = \frac{1}{30} f^G_{-2} - \frac{13}{60} f^G_{-1} + \frac{47}{60} f^G_0 + \frac{27}{60} f_1 - \frac{1}{20} f_2 \tag{19}$$

$$j = 1, \ldots, N-1:$$

$$\frac{3}{10}\hat{f}_{j-1/2} + \frac{6}{10}\hat{f}_{j+1/2} + \frac{1}{10}\hat{f}_{j+3/2} = \frac{1}{30} f_{j-1} + \frac{19}{30} f_j + \frac{1}{3} f_{j+1} \tag{20}$$

$$j = N:$$

$$\hat{f}_{N+1/2} = \frac{1}{30} f_{N-2} - \frac{13}{60} f_{N-1} + \frac{47}{60} f_N + \frac{27}{60} f^G_{N+1} - \frac{1}{20} f^G_{N+2} \tag{21}$$

where the superscript G denotes ghost points. The conserved variables at the ghost points are specified in a manner consistent with the physical boundary conditions and the corresponding fluxes are known. Thus, the complete numerical scheme can be expressed as:

$$\mathrm{A}\hat{\mathbf{f}} = \mathrm{B}\mathbf{f} + \mathbf{b} \tag{22}$$

where

$$\mathrm{A} = \begin{bmatrix} 1 & & & & & & \\ \frac{3}{10} & \frac{6}{10} & \frac{1}{10} & & & & \\ & \frac{3}{10} & \frac{6}{10} & \frac{1}{10} & & & \\ & & \ddots & \ddots & \ddots & & \\ & & & \frac{3}{10} & \frac{6}{10} & \frac{1}{10} & \\ & & & & & 1 \end{bmatrix}, \quad \mathrm{B} = \begin{bmatrix} \frac{27}{60} & -\frac{1}{20} & & & & & \\ \frac{19}{30} & \frac{1}{3} & & & & & \\ \frac{1}{30} & \frac{19}{30} & \frac{1}{3} & & & & \\ & \ddots & \ddots & \ddots & & & \\ & & & \frac{1}{30} & \frac{19}{30} & \frac{1}{3} & \\ & & & \frac{1}{30} & -\frac{13}{60} & \frac{47}{60} & \end{bmatrix} \tag{23}$$

and the boundary terms are given by

$$\mathbf{b} = \begin{bmatrix} \frac{1}{30} f_{-2}^G - \frac{13}{60} f_{-1}^G + \frac{47}{60} f_0^G \\ \frac{1}{30} f_0^G \\ \vdots \\ \frac{27}{60} f_{N+1}^G - \frac{1}{20} f_{N+2}^G \end{bmatrix} \tag{24}$$

Numerical analysis of the CRWENO scheme with this boundary closure is presented in [21] and it is verified that this implementation is numerically stable.

3 Numerical Properties

The numerical properties of the CRWENO5 scheme with the various non-linear weights are analyzed and discussed in this section. The truncation errors, spectral properties and resolution of discontinuities are studied for the linear advection equation. A theoretical analysis of (8), which is the underlying linear scheme for the fifth-order CRWENO scheme, was presented in [20,21] and the fifth-order linear compact scheme was compared with the fifth-order linear non-compact scheme (which corresponds to the WENO5 scheme). Although numerical tests on the linear advection equation and the inviscid Euler equations agreed well with the conclusions from the linear analysis, the non-linearity of the CRWENO5 (and WENO5) scheme can have significant effect on the numerical properties [26], even when applied to linear problems. This section investigates this effect for the various formulations of the non-linear weights in the context of the CRWENO5 scheme and quantifies the numerical properties of the non-linear scheme.

Taylor series analysis of the linear, fifth-order compact scheme (8), henceforth referred to as "Compact5", show that its leading dissipation and dispersion errors are, respectively, $1/10$-th and $1/15$-th those of the fifth-order non-compact scheme. Thus, for the same order of convergence, the CRWENO5 scheme yields solutions with significantly lower truncation errors. This is verified and demonstrated in [20] through the application of the CRWENO5 and WENO5 schemes to a smooth problem, for which the CRWENO5 and WENO5 schemes reduce to their linear counterparts. In this paper, the effects of the non-linear weights on the accuracy and convergence for a smooth problem with vanishing derivatives are studied with the following initial solution:

Table 2 L_2 errors, convergence rates (for 1 cycle) and runtimes (100 cycles) for CRWENO5 schemes with the various formulations for the non-linear weights

N	$\epsilon = 10^{-6}$		$\epsilon = 10^{-20}$		Runtime (s)
	Error	r_c	Error	r_c	
CRWENO5-JS					
20	3.825E−03	–	3.825E−03	–	4.264E−01
40	2.172E−04	4.14	2.174E−04	4.14	2.214E+00
80	1.082E−05	4.33	1.096E-05	4.31	1.312E+01
160	6.178E−07	4.13	7.059E−07	3.96	8.244E+01
320	2.089E−08	4.89	5.266E−08	3.74	6.327E+02
CRWENO5-M					
20	6.785E−04	–	6.786E−04	–	5.211E−01
40	1.387E−05	5.61	1.388E−05	5.61	2.924E+00
80	3.649E−07	5.25	3.659E−07	5.25	1.773E+01
160	1.061E−08	5.10	1.069E−08	5.10	1.127E+02
320	3.229E−10	5.04	3.242E−10	5.04	7.099E+02
CRWENO5-Z					
20	1.312E−03	–	1.313E−03	–	4.972E−01
40	2.336E−05	5.81	2.342E−05	5.81	2.702E+00
80	4.430E−07	5.72	4.511E−07	5.70	1.613E+01
160	1.085E−08	5.35	1.147E−08	5.30	1.048E+02
320	3.229E−10	5.07	3.324E−10	5.11	6.800E+02
CRWENO5-YC					
20	4.530E−04	–	4.529E−04	–	4.738E−01
40	1.226E−05	5.21	1.226E−05	5.21	2.849E+00
80	3.528E−07	5.12	3.528E−07	5.12	1.612E+01
160	1.056E−08	5.06	1.059E−08	5.06	1.134E+02
320	3.229E−10	5.03	3.229E−10	5.03	6.481E+02

$$u_0(x) = \sin\left(\pi x - \frac{\sin(\pi x)}{\pi}\right), \tag{25}$$

on a periodic domain $-1 \leq x \leq 1$. Solutions are obtained after one cycle with the CRWENO5 schemes listed in Table 1 on different grids. The initial CFL is 0.1 for the 20-point grid and is reduced by a factor of $2/(2^{5/3})$ at each refinement to ensure that the errors due to time discretization converge at the same rate as those due to the spatial discretization. A low CFL number is chosen to ensure that the errors due to time discretization are significantly lower than those due to space discretization. Table 2 shows the L_2 error norms and the rates of convergence (r_c) after 1 cycle and the total run-times after 100 cycles for the two different ϵ values (10^{-6} and 10^{-20}). The CRWENO5-JS scheme shows sub-optimal convergence for this problem and this agrees with the behavior of the WENO5-JS scheme for this problem [23]. It should be noted that, unlike the WENO5-JS scheme, the CRWENO5-JS schemes shows poor convergence for both ϵ-values; the non-linear errors are exacerbated on the finer meshes for $\epsilon = 10^{-20}$. The other formulations for the weights recover the optimal order of convergence; however, CRWENO5-M and CRWENO5-Z show significant irregularities on the coarser meshes. The errors approach similar values on finer meshes and the schemes show fifth-order convergence, especially for $\epsilon = 10^{-6}$, indicating that the weights are at their

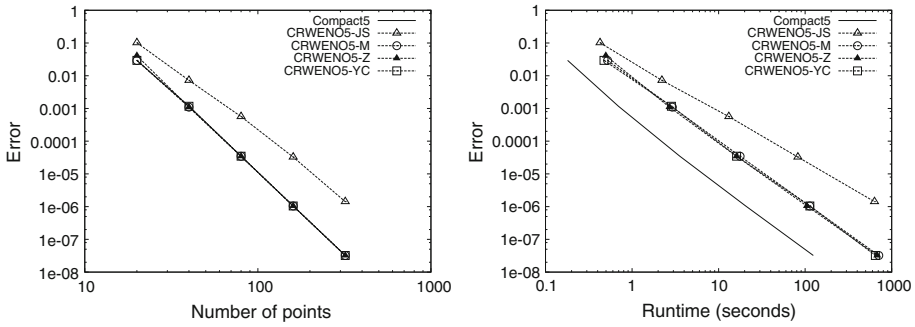

Fig. 3 L_2 error norms as functions of number of grid points and run-time for $\epsilon = 10^{-6}$. **a** Grid convergence, **b** numerical cost

optimal values. The CRWENO5-YC scheme yields solutions with the lowest errors at all grid sizes. In addition, the errors are insensitive to the value of ϵ for all the grid sizes considered. Figure 3a shows the L_2 error norms after 100 cycles as a function of the number of grid points with $\epsilon = 10^{-6}$ for the CRWENO5 schemes as well as the linear Compact5 scheme. While the CRWENO5-JS scheme shows sub-optimal convergence and yields solutions with higher errors than the Compact5 scheme, solutions obtained from the CRWENO5-M, CRWENO5-Z and CRWENO5-YC schemes have identical errors as the linear scheme.

Table 2 shows that the run-times for the CRWENO5-M scheme are substantially higher than those of the CRWENO5-JS scheme at the same grid size due to the evaluation of the mapping function. The CRWENO5-Z and CRWENO5-YC schemes reformulate the weights but need the computation of the τ parameter. Thus, their run-times are higher than those of the CRWENO5-JS scheme but significantly lower than the CRWENO5-M scheme. Figure 3b shows the errors as a function of the runtime for the CRWENO5 schemes and the linear Compact5 scheme. It is observed that although these alternative formulations of the non-linear weights introduce a numerical overhead to the WENO algorithm, the reduction in error justifies the additional expense. The CRWENO5-M, CRWENO5-Z and CRWENO5-YC are computationally more efficient, yielding solutions with lower errors for the same runtime (or solutions with comparable errors at a lower numerical cost).

A Fourier analysis of (8) was presented in [20] and it was shown that the fifth-order compact scheme has significantly lower dispersion and dissipation over a larger range of wavenumbers than the fifth-order non-compact scheme that corresponds to the WENO5 scheme. The spectral properties compared favorably to the linear equivalents of several high-resolution, non-oscillatory schemes proposed in the literature, including the bandwidth-optimized WENO schemes [30,31] and weighted compact non-linear schemes [17]. The improved spectral resolution of the CRWENO5 scheme was demonstrated on the linear advection equation and the inviscid Euler equations. Although the numerical solutions to problems with high wavenumbers and discontinuities agreed well qualitatively with the conclusions drawn from the linear analysis, the non-linear WENO mechanism has a significant effect on the spectral properties, especially for solutions with moderate and higher wavenumbers. Thus, quantifying the non-linear effects on the performance of the CRWENO5 scheme is required to understand its behavior for compressible, turbulent flows.

An approximate dispersion relation was proposed [26] that constructs the dispersion relationship for a non-linear scheme through a series of numerical tests where an initial solution

with an assigned wavenumber is convected over a very small distance (to reduce time-integration induced errors). For each wavenumber in the grid-supported range, the final solution is analyzed to obtain the dispersion and dissipation at that wavenumber for the non-linear scheme. Differences were observed in the dispersion relationship of the WENO5 scheme and that of its linear counterpart, especially at moderate and high wavenumbers, demonstrating the effect of the non-linear weights on the spectral properties. However, one major drawback of this analysis is that by considering one wavenumber at a time, the non-linear interactions between the different wavenumbers is not captured. An improved non-linear spectral analysis was proposed [27] where the dispersion and dissipation relations are obtained by analyzing the numerical derivative of a solution with all supported wavenumbers. The phase for each wavenumber is random and the amplitude is specified such that the energy spectrum corresponds to the turbulent energy spectrum. Several realizations of the solution are taken to obtain statistically relevant spectral properties.

In this paper, we consider the non-linear spectral analysis [27] to quantify the effects of the non-linear weights on the CRWENO5 scheme. The non-linear analyses in [26,27] demonstrate the effect of the non-linearity on the spectral properties of the WENO5 scheme (among other shock-capturing schemes); however they did not consider the alternative formulations for the non-linear weights discussed in the previous section. Thus, in addition to the CRWENO5 scheme, we study the non-linear spectral properties of the WENO5 scheme in this section. The solution is expressed as

$$u_0(j) = \sum_{k=1}^{N/2} A(k)\cos\left[2\pi j(k\Delta x) + \phi(k)\right];\ j = 1, \ldots, N;\ -\pi \le \phi(k) < \pi, \qquad (26)$$

on a periodic domain $x \in [-1, 1]$. The amplitude is $A(k) = k^{-5/6}$ such that the energy corresponds to the $E(k) \propto k^{-5/3}$ turbulent flow energy distribution. Figure 4 shows the dispersion and dissipation as a function of the wavenumber for the WENO5-JS, CRWENO5-JS schemes, and the fifth-order linear compact (Compact5) and non-compact (NonCompact5) schemes (note that the NonCompact5 scheme is the linear counterpart of the WENO5 scheme). The spectral properties shown for the non-linear schemes are averaged over 50, 000 realizations

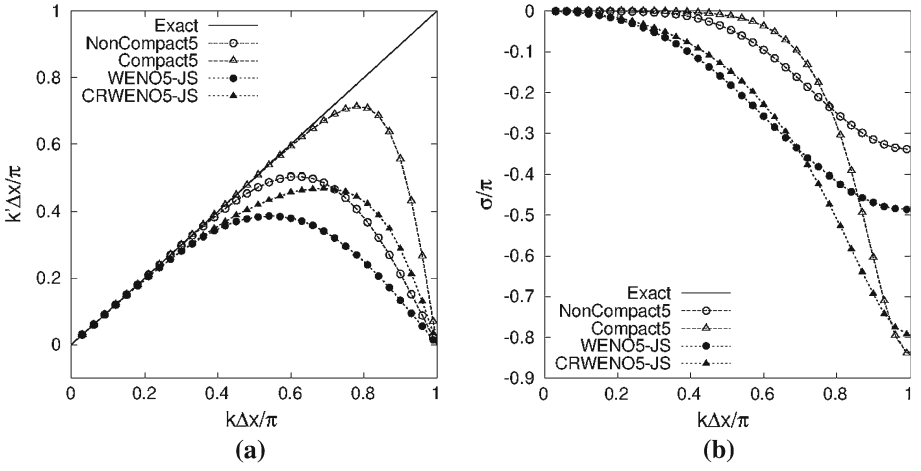

Fig. 4 Non-linear spectral properties of the linear fifth-order, WENO5-JS and CRWENO5-JS schemes. **a** Dispersion, **b** dissipation

of the random initial solution prescribed in (26). The Compact5 scheme resolves a significantly larger range of wavenumbers than the NonCompact5 scheme and the dissipation of the Compact5 scheme is significantly lower than the NonCompact5 scheme for low and moderate wavenumbers. At high wavenumbers, the dissipation of the Compact5 scheme is higher than that of the NonCompact5 scheme; however this is actually advantageous as these wavenumbers are incorrectly resolved (as observed from the dispersion characteristics). The non-linear weights have a significant degrading effect on the spectral properties of both the WENO5 and CRWENO5 schemes. However, it is observed that even after accounting for the non-linear effects, the CRWENO5 scheme has a significantly higher spectral resolution than the WENO5 scheme and the conclusions drawn from the linear schemes are qualitatively true for the non-linear schemes as well.

Figures 5 and 6 show the averaged dispersion and dissipation, respectively, of the CRWENO5 and the WENO5 schemes with the various formulation of the non-linear weights. The alternative formulations improve the spectral resolution of both these schemes compared to the original formulation of the weights. The WENO5-Z and WENO5-YC schemes show the highest spectral resolution amongst the WENO5 schemes, while the mapped weights yield the highest spectral resolution for the CRWENO5 schemes. While the WENO5-M, WENO5-Z and WENO5-YC schemes have significantly lower dissipation at moderate and higher wavenumbers compared to the WENO5-JS scheme, the various formulations of the non-linear weights result in similar dissipation characteristics for the CRWENO5 schemes. The averaged dispersion and dissipation show the overall effect of the non-linearity on the numerical scheme; in addition, the standard deviation (σ) shows the sensitivity of the non-linear weights to the various realizations of the random solution. Figure 7 shows the dispersion as a function of the wavenumber with the σ-band for each of the WENO5 schemes. In addition to improved averaged spectral resolution, the WENO5-Z and WENO5-YC have significantly lower standard deviations, indicating that the non-linear weights are not as erratic as for the WENO5-JS scheme. The WENO5-M scheme, however, shows a similar standard deviation as the WENO5-JS and this is expected since the weights are initially computed using original formulation and then mapped. Figure 8 shows the dispersion with

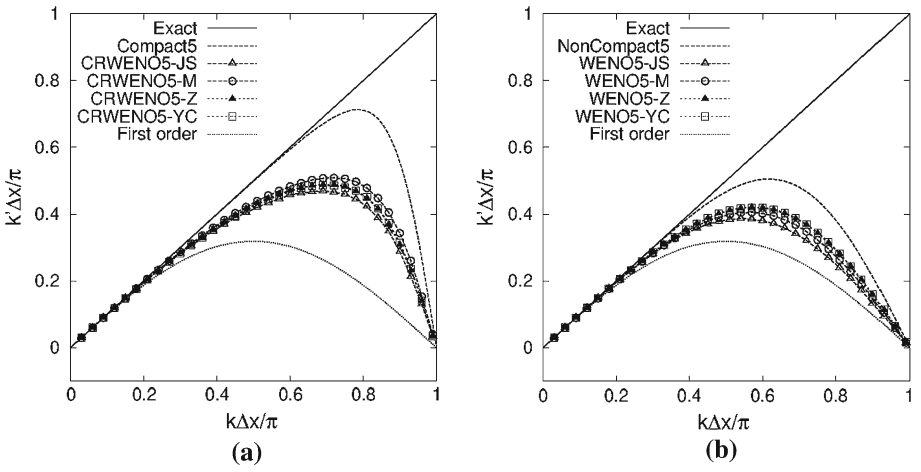

Fig. 5 Dispersion properties of the CRWENO5 (**a**) and WENO5 (**b**) with the various formulations for the non-linear weights.

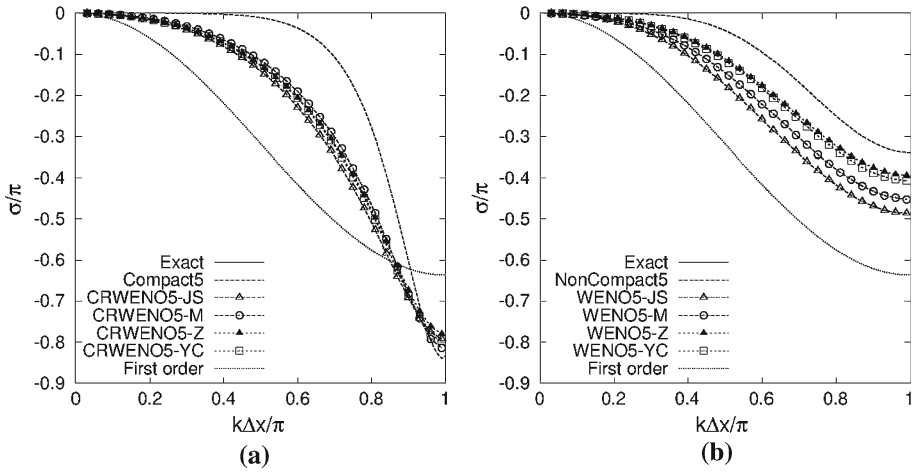

Fig. 6 Dissipation properties of the CRWENO5 (**a**) and WENO5 (**b**) with the various formulations for the non-linear weights

the σ-bands for the CRWENO5 schemes. Unlike the WENO5 scheme, the CRWENO5-Z and CRWENO5-YC schemes show the same standard deviation as the CRWENO5-JS and CRWENO5-M schemes, indicating that the non-linear weights are just as sensitive to the solution. The various non-linear weights considered in this paper were all formulated for the non-compact WENO5 scheme, and thus, some of their properties are lost when applied to the CRWENO5 scheme. However, it can be concluded that they do provide a non-linear mechanism that ensures high-order accuracy for smooth solutions and non-oscillatory behavior across discontinuities. The alternative formulations [23–25] for the weights show significant benefits for the CRWENO5 scheme over the original formulation of Jiang and Shu [2].

Finally, the behavior of the weights is analyzed for a problem consisting of several discontinuous waves. The initial solution consists of exponential, square, triangular and parabolic waves and is given by

$$u_0(x) = \begin{cases} \exp\left(-\log(2)\frac{(x+7)^2}{0.0009}\right) & \text{if} \quad -0.8 \le x \le -0.6, \\ 1 & \text{if} \quad -0.4 \le x \le -0.2, \\ 1 - |10(x-0.1)| & \text{if} \quad 0 \le x \le 0.2, \\ \left[1 - 100(x-0.5)^2\right]^{1/2} & \text{if} \quad 0.4 \le x \le 0.6, \\ 0 & \text{otherwise} \end{cases} \tag{27}$$

over the periodic domain $-1 \le x \le 1$. Solutions are obtained after 50 cycles, and the exponential and square waves are shown in Fig. 9. While the CRWENO5-JS schemes shows significant dissipation, the alternative implementation of the weights improve the resolution of the solution. The solution obtained using the CRWENO5-YC scheme shows the least dissipation and phase error. Figure 10 shows the three weights ($\omega_{1,2,3}$) over the domain for the various schemes. The weights computed by the CRWENO5-JS scheme are far from optimal throughout the domain. The mapping function causes the weights to converge more rapidly to their optimal values and this is observed for the weights

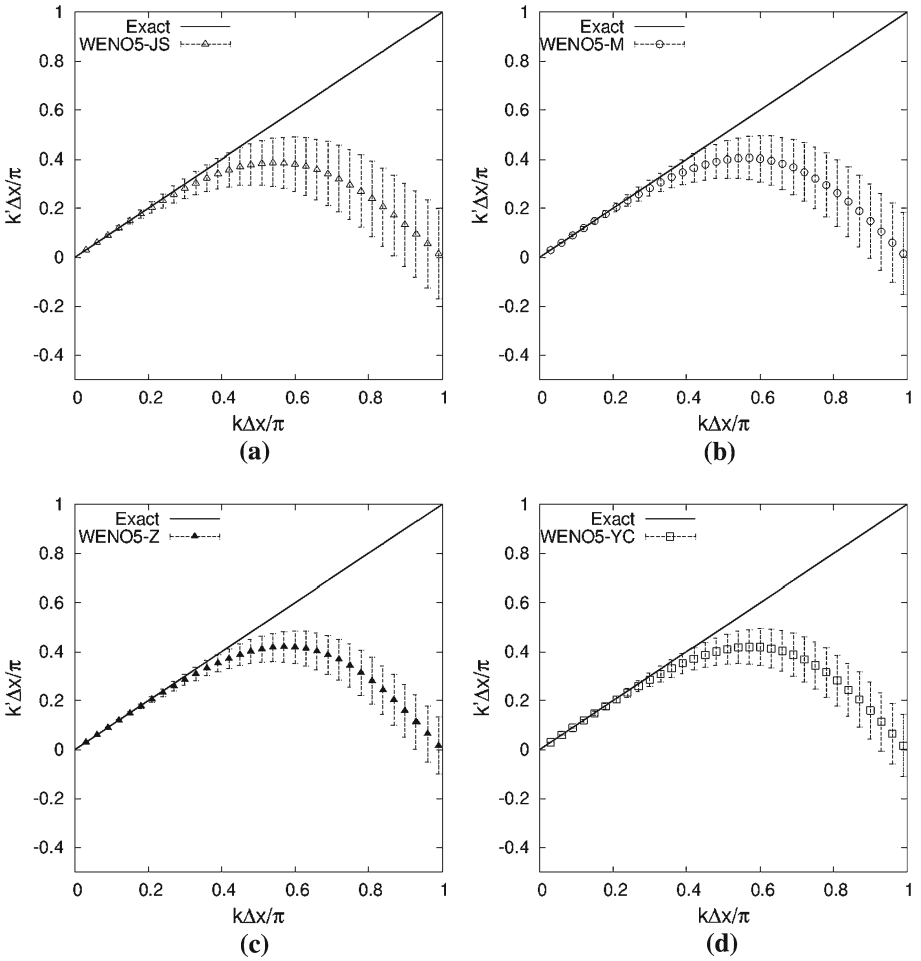

Fig. 7 Average dispersion and standard deviation for the WENO5 schemes. **a** WENO5-JS, **b** WENO5-M, **c** WENO5-Z, **d** WENO5-YC

computed by CRWENO5-M. A similar observation is made for the CRWENO5-Z with the computed weights being nearer to their optimal values compared to the CRWENO5-JS scheme. The weights computed by the CRWENO5-YC scheme are observed to be the closest to their optimal values in the smooth regions of the solution. The weights for stencils containing the discontinuities go to zero at the discontinuity with minimal smearing.

4 Application to the Euler Equations

The CRWENO schemes are applied to the Euler equations in this section and the effects of the non-linear weights are studied for inviscid flow problems representative of compressible, turbulent flows. The Euler equations are a hyperbolic system of PDEs and the extension of scalar interpolation schemes to this system was presented in [20]. The application of (9) to the

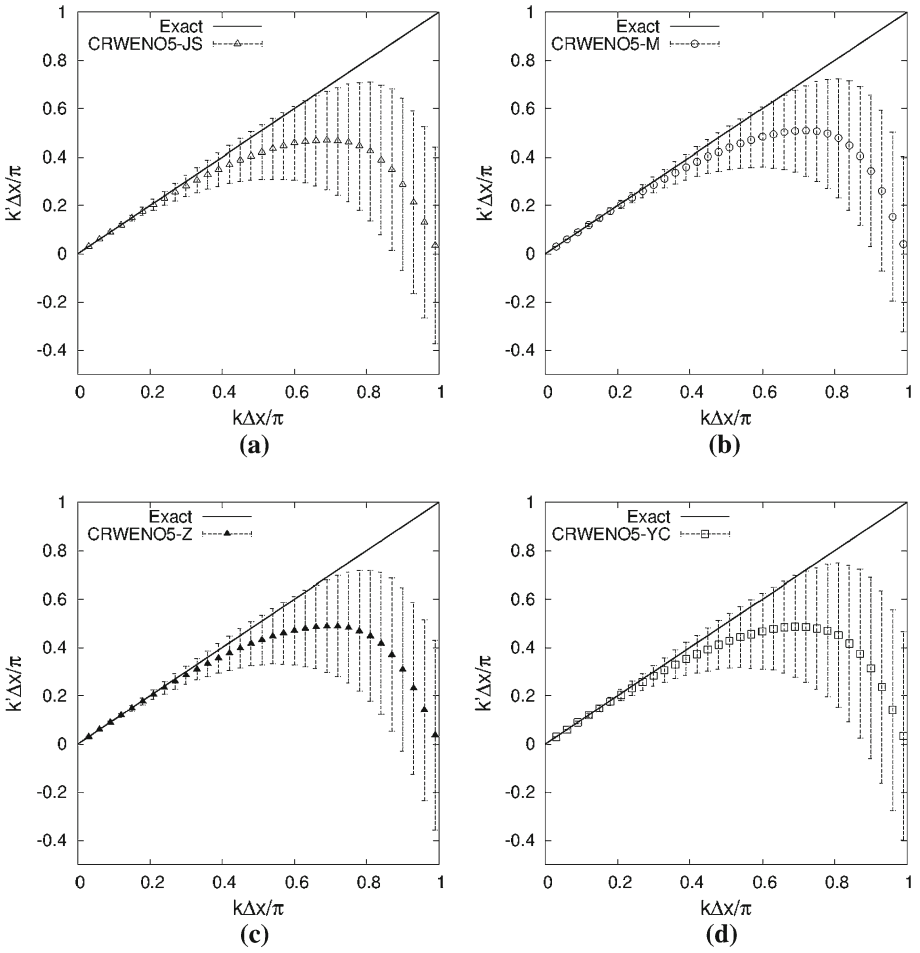

Fig. 8 Average dispersion and standard deviation for the CRWENO5 schemes. **a** CRWENO5-JS, **b** CRWENO5-M, **c** CRWENO5-Z, **d** CRWENO5-YC

reconstruction of primitive (density, velocity and pressure) and conserved variables (density, momentum and energy) is trivial since these scalar quantities can be interpolated independently of each other. A characteristic-based reconstruction applies (9) to the characteristic fluxes, and thus, the components of the unknown flux vector are coupled through the matrix of left eigenvectors. This requires solving a block tridiagonal system of equations, which is more expensive than the solution to a tridiagonal system. The computational efficiency of these schemes was studied [20,21] and it was observed that while the CRWENO5 scheme is more efficient than the WENO5 scheme for the reconstruction of conserved and primitive variables, it is not so for a characteristic-based reconstruction. The reconstruction of characteristic variables is required to yield robust, non-oscillatory solutions for inviscid flow problems with strong shocks [2]. However, several examples [22] show that for realistic flow problems with physical viscosity present, the reconstruction of conserved or primitive variables is sufficient to yield accurate solutions. Thus, this drawback of the CRWENO5 scheme does not limit its applicability to subsonic and transonic turbulent flows. The inviscid flow

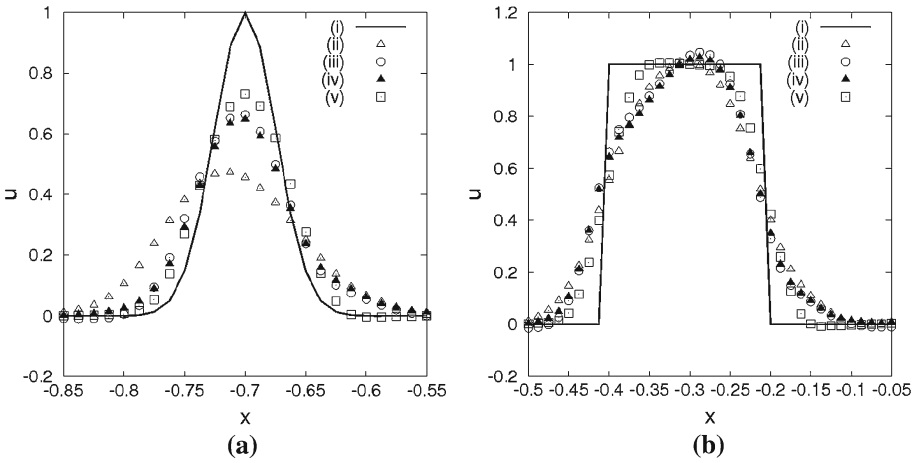

Fig. 9 Comparison of CRWENO5 schemes with the various non-linear weights for a discontinuous solution: (*i*) Exact Solution, (*ii*) CRWENO5-JS, (*iii*) CRWENO5-M, (*iv*) CRWENO5-Z, (*v*) CRWENO5-YC. **a** Exponential wave after 50 cycles, **b** Square wave after 50 cycles

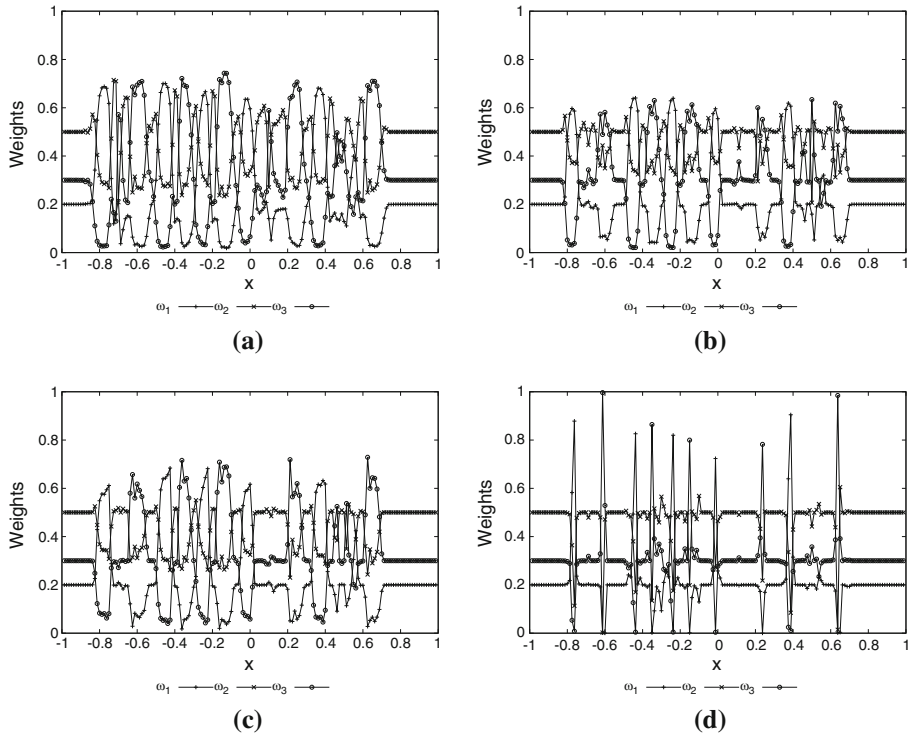

Fig. 10 Comparison of the weights for a discontinuous solution after one cycle. **a** CRWENO5-JS, **b** CRWENO5-M, **c** CRWENO5-Z, **d** CRWENO5-YC

problems in this section are solved using a characteristic-based reconstruction to demonstrate the numerical properties of the CRWENO5 schemes. These numerical properties extend to viscous flow problems where the conserved or primitive variables are reconstructed.

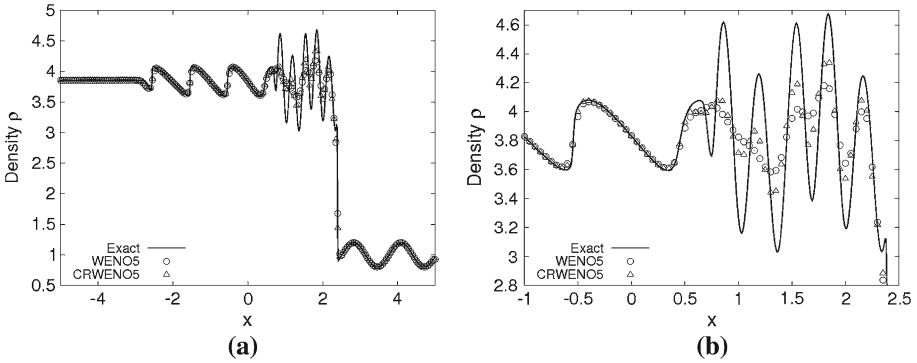

Fig. 11 Solutions to the shock—entropy wave interaction problem. **a** Complete solution, **b** Discontinuities and small length-scale waves

4.1 Shock: Entropy Wave Interaction

The interaction of a shock wave with an entropy wave [29] results in the formation of discontinuities and small-length-scale waves, and is a simplified one-dimensional representation of compressible turbulent flows. The initial conditions consist of a Mach 3 shock wave and a density wave and are expressed as

$$(\rho, u, p) = \begin{cases} \left(\frac{27}{7}, \frac{4\sqrt{35}}{9}, \frac{31}{3}\right) & \text{if } x < -4 \\ \left(1 + \frac{1}{5}\sin 5x, 0, 1\right) & \text{if } x \geq -4 \end{cases} \tag{28}$$

The domain is $[-5, 5]$ and zero-gradient boundary conditions are enforced at both boundaries. Solutions are obtained at $t = 1.8$ at a CFL of 0.1 on a grid with 200 points. Figure 11 shows the solution (density) obtained by the CRWENO5 and WENO5 scheme with the original formulation [2] for the non-linear weights. ("Exact Solution" refers to the solution obtained by the WENO5 scheme on a grid with 2000 points). The CRWENO5 scheme shows an improved resolution of the small length scales compared to the WENO5 scheme, while maintaining non-oscillatory behavior across the discontinuities. This is due to the higher spectral resolution of the underlying linear scheme.

The effect of the non-linear weights is studied and Fig. 12 shows the solutions obtained by the various formulations of the weights for the CRWENO5 scheme. The alternative formulations for the weights show significant improvements in the resolution of the small length scales, compared to the CRWENO5-JS scheme. This is explained by observing the weights in the post-shock region, shown in Fig. 13. The region containing the small-length-scale density waves is shown. The density waves correspond to the characteristic field with eigenvalue u and the corresponding weights are shown for a left-biased reconstruction (the behavior is similar for the right-biased reconstruction). The weights computed using the CRWENO5-JS implementation show significant deviations from the optimal values, thus treating the smooth solution as discontinuities and introducing excessive dissipation. The mapped weights (CRWENO5-M) are closer to their optimal values. The CRWENO5-Z and CRWENO5-YC implementations show significant improvements in the weights resulting in superior resolution of the solution.

It is thus demonstrated that the implementation of the non-linear weights has a significant effect on the smaller length scales in the solution. While the CRWENO5 scheme improves

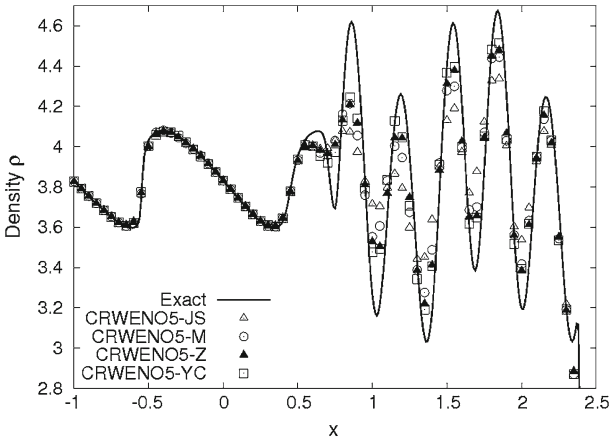

Fig. 12 Solutions to the shock—entropy wave interaction problem with various implementations of non-linear weights

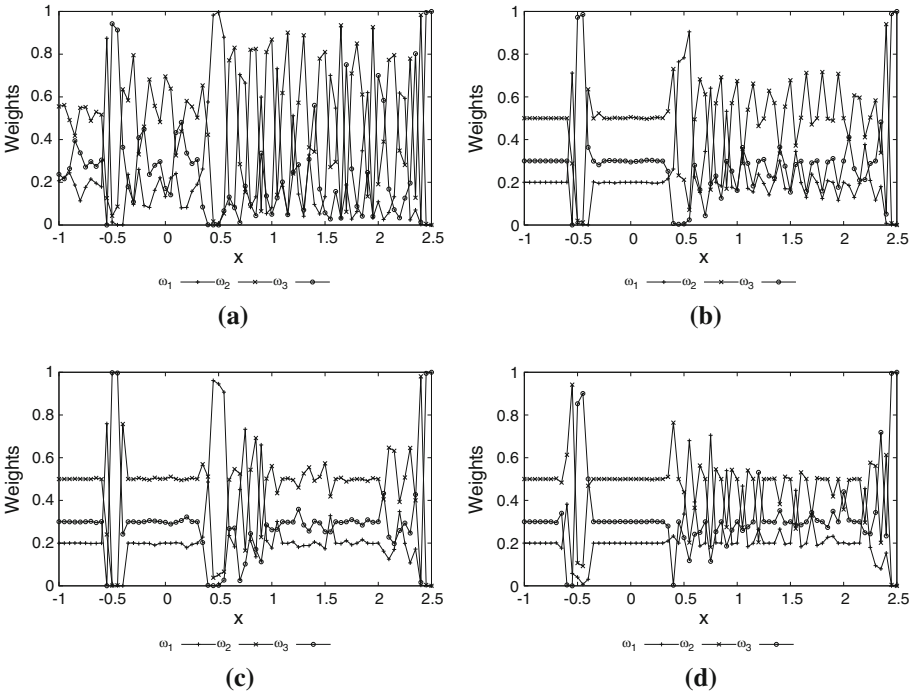

Fig. 13 Shock—entropy wave interaction: Weights for the left-biased reconstruction of characteristic field u ($\epsilon = 10^{-6}$). **a** CRWENO5-JS, **b** CRWENO5-M, **c** CRWENO5-Z, **d** CRWENO5-YC

upon the performance of the WENO5 scheme by replacing the underlying linear scheme with a compact interpolation scheme, further improvements are obtained by the alternative formulations for the non-linear weights. Similar improvements have also been reported with the WENO5 scheme for this problem [23–25]

4.2 Shock: Vorticity Wave Interaction

The interaction of a shock wave with a vorticity wave [29] is a two-dimensional, simplified representation of shock-turbulence interactions and requires the accurate capturing of acoustic, vorticity and entropy waves. Hybrid compact-ENO/WENO schemes have been applied to this problem in previous studies [14,15]. The domain is $[-1.5, 1.5] \times [-1, 1]$. The initial conditions comprise a Mach 8 shock (located at $x = -1$) and a vorticity wave specified upstream of the shock as:

$$\begin{aligned} \rho &= 1, \ p = 1 \\ u &= -\sqrt{\gamma}\sin\theta\cos\left(2\pi x\cos\theta + 2\pi y\sin\theta\right), \\ v &= \sqrt{\gamma}\cos\theta\cos\left(2\pi x\cos\theta + 2\pi y\sin\theta\right), \end{aligned}$$

where $\theta = \pi/6$ is the angle of the vorticity wave with the shock wave. Uniform post-shock conditions are specified downstream of the shock. Periodic boundary conditions are enforced on the top and bottom boundaries ($y = \pm 1$). Steady flow values corresponding to the flow conditions upstream and downstream of the shock are specified at the left and right boundaries ($x = \pm 1.5$). The solution is evolved to a time of $t = 0.2$ at a CFL number of 0.5.

Solutions are obtained at two different grid sizes—96×64 and 192×128. Figure 14 shows the density and out-of-plane vorticity contours for the solution obtained by the CRWENO5 scheme on the 192×128 grid. The solutions show good agreement with those in the literature [14,15,29]. Figure 15a shows the density through $y = 0$, magnified around the post-shock region. The "exact" solution is obtained with the WENO5 scheme on a 960×640 grid. The solution consists of fast left-running acoustic waves and slow left-running entropy and vorticity waves, demarcated by a discontinuity near $x = 0.55$. The CRWENO5 scheme shows a sharper resolution of the solution at both grid refinement levels than the WENO5 scheme. The effect of the non-linear weights on the numerical solution is analyzed and Fig. 15b shows the cross-sectional density for the solutions obtained by the different CRWENO5 schemes. This problem does not consist of very small length scales and thus, improvements with alternative formulations for the weights are very slight. It should be noted that the CRWENO-Z scheme shows significantly higher resolution for the entropy and vorticity waves; however it also suffers from slight oscillations across the shock leading the acoustic waves.

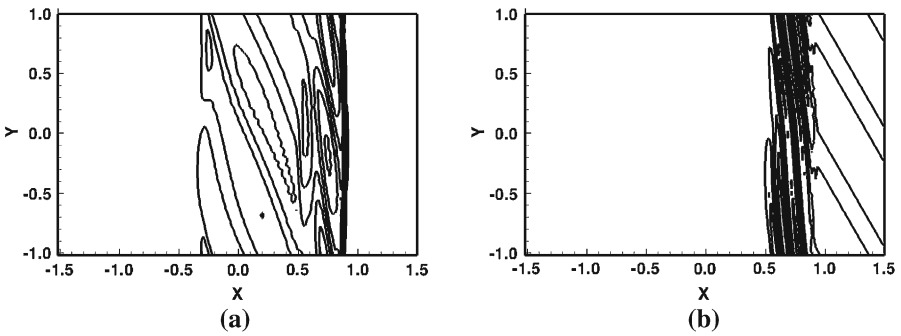

Fig. 14 Solution for the shock—vorticity wave interaction problem (192×128 grid). **a** Density—30 contour levels between 0.99 and 6.16, **b** vorticity—16 contour levels between -100 and 100

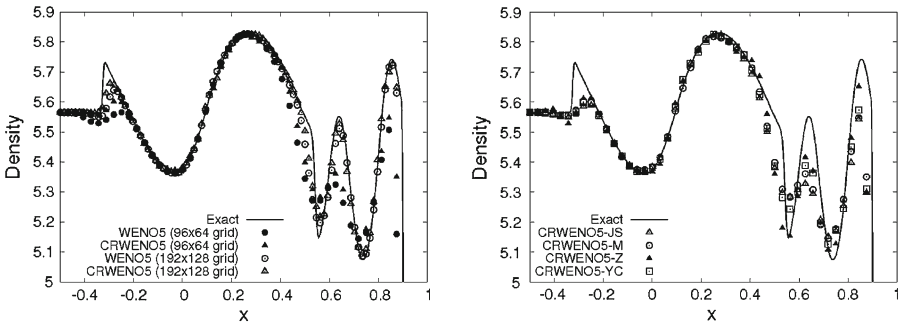

Fig. 15 Cross-sectional density for shock—vorticity wave interaction problem. **a** Comparison of the CRWENO5 and WENO5 schemes, **b** comparison of the various implementations of the weights for CRWENO5 scheme (96×64 grid)

5 Application to Compressible, Turbulent Flows

The DNS of compressible, turbulent flows requires a non-oscillatory numerical scheme with high spectral resolution. The numerical properties of the CRWENO5 scheme, as demonstrated in [20] and in the previous sections, make them suitable candidates to solve such flows. Two canonical problems—isotropic turbulence decay and the shock-turbulence interaction—are attempted in this section and the three-dimensional Navier–Stokes equations are solved without any turbulence model. Solutions obtained by the CRWENO5 scheme are compared to those obtained by the WENO5 scheme. In addition, the effects of the different formulations for the non-linear weights are studied. A characteristic-based reconstruction renders the CRWENO5 scheme less efficient than the WENO5 scheme; therefore, in these examples, a component-wise reconstruction is used. The CRWENO5 scheme is computationally more efficient than the WENO5 scheme for a component-wise reconstruction [20] and in the presence of physical dissipation, such an approach is sufficient to yield robust solutions [22]. This is verified by solving the viscous, steady-state flow across a standing shock wave. The viscous terms are discretized using the fourth-order central difference scheme. The flow problems considered in this section are discretized on uniform Cartesian grids and thus, the viscous terms are integrated in time using the explicit TVD-RK3 scheme. Previous studies in the literature have applied bandwidth-optimized non-compact schemes [30–32] as well as compact-ENO/WENO schemes [14,15,38] to such flow problems.

5.1 Isotropic Turbulence Decay

The decay of three-dimensional, isotropic turbulence is characterized by an energy transfer to smaller length scales from a specified initial energy spectrum of turbulent fluctuations. The flow is compressible for strong velocity fluctuations and a non-oscillatory scheme is required to accurately capture the formation of shocklets. The initial conditions are random, isotropic velocity fluctuations satisfying a prescribed energy spectrum [33,34]

$$E(k) = 16\sqrt{\frac{2}{\pi}}\frac{u_0^2}{k_0}\left(\frac{k}{k_0}\right)^4 \exp\left[-2\left(\frac{k}{k_0}\right)^2\right], \tag{29}$$

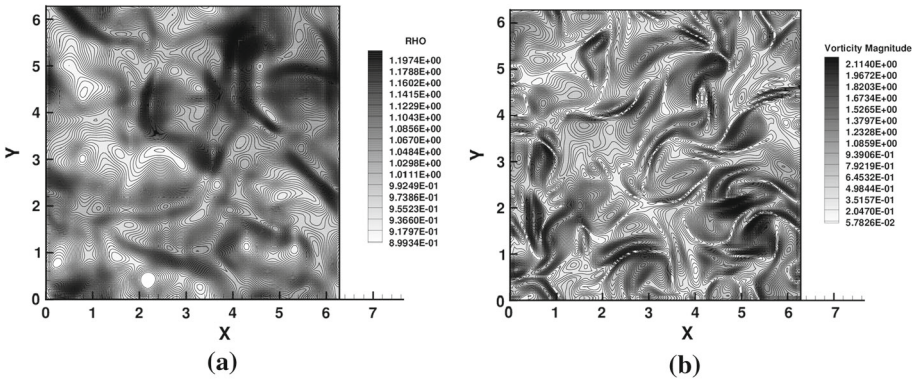

Fig. 16 Solution for the isotropic turbulence decay at $t/\tau = 3$ obtained by the CRWENO5-JS on a 128^3 grid. **a** Density **b** vorticity magnitude

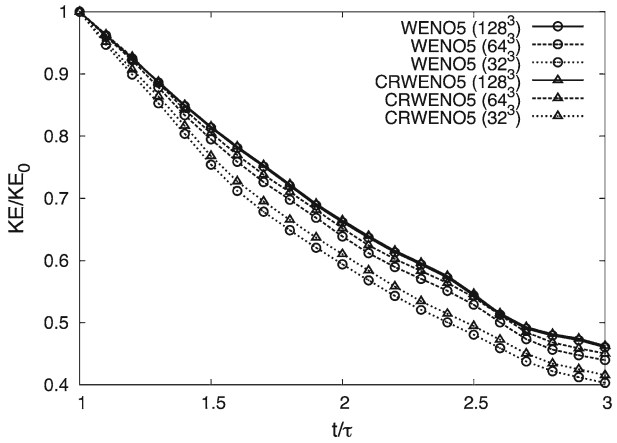

Fig. 17 Decay of kinetic energy: CRWENO5 and WENO5 schemes are various grid resolutions

where u_0 is the RMS turbulence intensity and k_0 is the wavenumber corresponding to the highest energy. The domain is taken as a cube of edge length 2π with periodic boundaries. The initial conditions are obtained by transforming the velocity fluctuations from the wavenumber space to the physical space and specifying constant density and pressure ($\rho = 1$, $p = 1/\gamma$) over the domain. In the present study, the flow is solved for $u_0 = 0.3$ and $k_0 = 4$ that results in a smooth, turbulent flow. Although shock structures are absent, the flow is characterized by strong gradients and this is shown in Fig. 16. The density and vorticity magnitude contours are shown for the solution obtained by the CRWENO5-JS scheme on a 128^3 grid. This example is used to demonstrate the effect of the non-linear weights for smooth flows with sharp gradients. Solutions are obtained at $Re_\lambda = 50$ where λ is the Taylor microscale.

The solutions are evolved till a final time of $t/\tau = 3.0$ where $\tau = \lambda/u_0$ is the turbulent time scale. The decay of the kinetic energy (non-dimensionalized by the initial kinetic energy) is shown in Fig. 17 for the WENO5 and CRWENO5 schemes at three different grid resolutions—32^3, 64^3 and 128^3. The original formulation for the non-linear weights, given in [2], is used to obtain these solutions. The solutions for the two schemes agree well at the

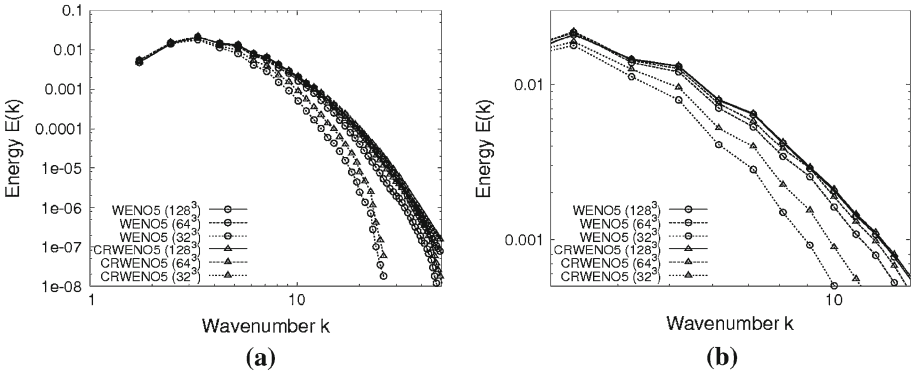

Fig. 18 Energy spectrum for the isotropic turbulence decay at $t/\tau = 2$. **a** Complete spectrum, **b** intermediate and small length scales

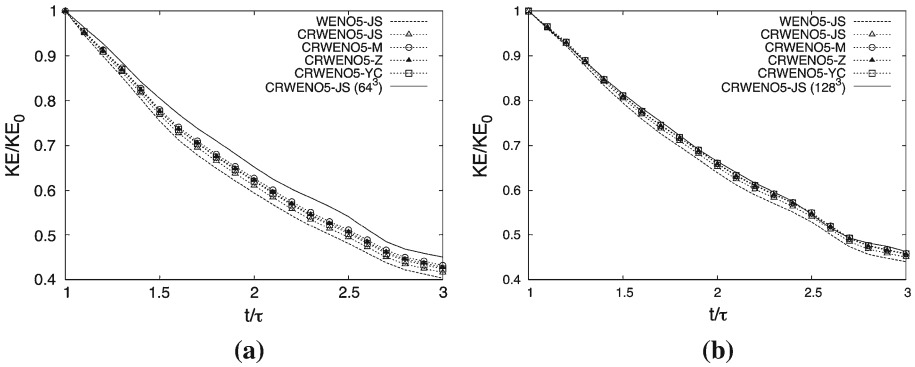

Fig. 19 Kinetic energy decay for various formulations of the non-linear weights. **a** 32^3 grid, **b** 64^3 grid

grid size of 128^3, indicating that both schemes yield similar solutions when the resolution is sufficient. The CRWENO5 scheme shows significantly lower dissipation than the WENO5 scheme at grid resolutions of 32^3 and 64^3. The energy spectrum at a time instant shows the resolution of the numerical solution as a function of length scales. Figure 18 shows the kinetic energy spectrum at $t/\tau = 2$. The solutions for the two schemes agree on the 128^3-point grid. At lower grid resolutions, the CRWENO5 scheme shows an improved resolution of higher wavenumbers (smaller length scales), compared to the WENO5 scheme.

The effect of the non-linear weights is explored for this flow problem. Figure 19 shows the kinetic energy decay for the solutions obtained by the various CRWENO5 schemes and the WENO5-JS on the 32^3 and 64^3 grids. The solution obtained by the CRWENO5-JS scheme on the finer grid is also included in each figure. While the baseline CRWENO5-JS schemes shows a significant improvement over the WENO5-JS scheme, further improvements are observed with the alternative formulations for the weights. The improvements are more visible for the 32^3 grid. Figure 20 shows the energy spectra for the solutions obtained by the various non-linear weights on the 32^3 grid. The alternative weights show a better resolution

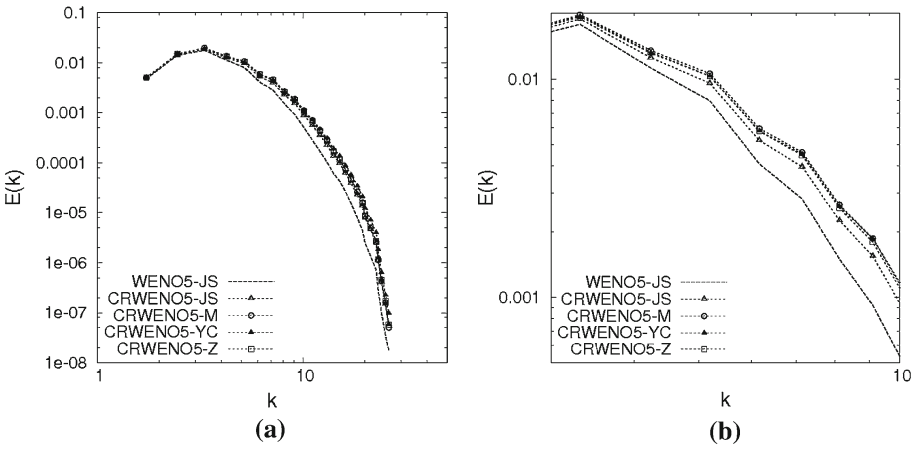

Fig. 20 Energy spectrum for various formulations of the non-linear weights (32^3 grid). **a** Complete spectrum, **b** magnified view

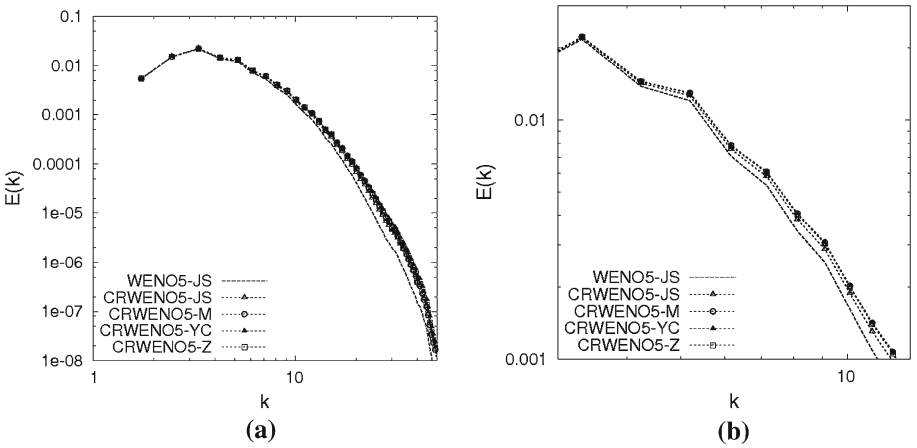

Fig. 21 Energy spectrum for various formulations of the non-linear weights (64^3 grid). **a** Complete spectrum, **b** magnified view

of the intermediate and smaller length scales. The energy spectra for the solutions obtained on the 64^3 grid is shown in Fig. 21 and similar conclusions may be drawn.

5.2 Shock-Turbulence Interaction

The interaction of an isotropic turbulent flowfield with a normal shock wave has been extensively studied [35–38] (and references therein) through the development of linear analysis as well as DNS. It has been observed that the interaction results in an amplification of turbulent fluctuations across the shock wave and a transfer of energy to smaller length scales. The domain is $[-2\pi, 2\pi] \times [0, 2\pi] \times [0, 2\pi]$ and discretized with a uniform grid. The flow is initialized as a stationary, Mach 2 shock at $x = 0$ with uniform upstream ($\rho = 1$, $u = M_s = 2$, $v, w = 0$, $p = 1/\gamma$ for $x < 0$) and downstream flow. Periodic boundary conditions are applied in the y and z directions. The sponge boundary treatment is applied at

the outflow boundary ($x = 2\pi$): the domain is extended in the flow direction beyond $x = 2\pi$ (sponge zone) and discretized with a stretched (along x) grid (with uniform spacing in the y and z directions). A sink term is added to the governing equations in this zone in the form of $\sigma(\mathbf{u} - \mathbf{u}_{ps})$ where $\mathbf{u}_{ps}$ is the uniform post-shock flow and σ varies linearly from 0 at $x = 2\pi$ to 1 at the downstream end of the sponge zone. A combination of grid-stretching and the sink term is sufficient to damp out the fluctuations and avoid reflections from the outflow boundary [39,40]. Characteristic-based outflow boundary conditions are applied at the downstream end of the sponge zone.

Inflow boundary conditions are enforced by adding a field of isotropic, turbulent fluctuations to the uniform, supersonic mean flow. The fluctuations are obtained from the solution to the decaying isotropic turbulence problem, discussed in the last section. Solenoidal velocity fluctuations, satisfying (29), with $u_0 = 0.3$ and $k_0 = 4$ are added to the mean supersonic inflow and numerically solved on a periodic domain of size $(2\pi)^3$ till $t/\tau = 1$. The density, velocity and pressure fluctuations are extracted from the mean flow and transformed from the (x, y, z)-space to the (t, y, z)-space through $x = M_s t$. These fluctuations are added to the uniform supersonic inflow. This procedure is described in more details in [41,42]. The procedure described here results in a periodic inflow with a time period of $2\pi/M_s$ while the procedure described in the references include a random "jitter" during each time period to remove this periodicity. Since the focus of this work is the performance and comparison of numerical schemes and not the flow physics, the jitter is not used. The simulations are run till a large non-dimensional time (t/τ) to ensure that statistically relevant quantities are obtained.

Solutions are obtained on two grids—$64 \times 32 \times 32$ (and $16 \times 32 \times 32$ points in the sponge zone) and $128 \times 64 \times 64$ (and $32 \times 64 \times 64$ points in the sponge zone), at a Taylor microscale Reynolds number of $Re_\lambda = 50$. Figure 22 shows the domain and the solution obtained by the CRWENO5 scheme on the fine grid. The isosurfaces of the second invariant of the velocity gradient tensor are shown. The figure also shows the $x - z$ cross-section of the mesh, especially the sponge zone with the stretched mesh. It is observed that the turbulent fluctuations are damped out successfully in the sponge zone due to a combination of the grid-stretching and the sink term.

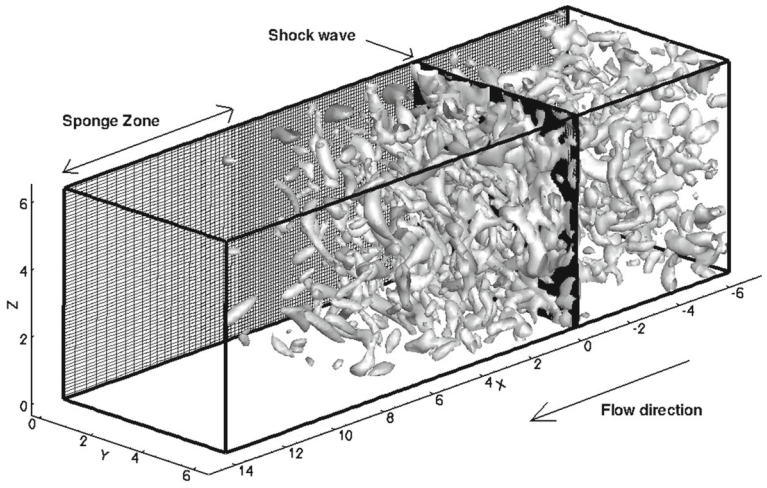

Fig. 22 Solution of the shock-turbulence interaction problem obtained by the CRWENO5 on a $128 \times 64 \times 64$ grid: Iso-surfaces of the second invariant of the velocity gradient tensor

The streamwise variation of density and pressure fluctuations is shown in Fig. 23 for the solutions obtained by the WENO5-JS scheme and the various CRWENO5 schemes on the $64 \times 32 \times 32$ grid. These statistical quantities are obtained by averaging in time and the cross-flow directions (y and z). An initial transient is observed in the fluctuations near the inflow boundary during which the turbulent flow-field develops from the prescribed inflow fluctuations. The interaction with the shock wave amplifies the turbulent fluctuations and this is observed for all the schemes. The CRWENO5-JS scheme predicts stronger fluctuations than the WENO5-JS upstream and downstream of the shock. The alternative formulations for the non-linear weights reduce the dissipation further, and are thus better able to capture the fluctuations. The mapped weights (CRWENO5-M) shows an improvement over the original weights (CRWENO5-JS), however, the CRWENO5-Z and CRWENO5-YC schemes yield solutions with the minimum dissipation for this problem. These differences are larger downstream of the shock wave. Figure 24 shows the density and pressure fluctuations for the solutions obtained on the $128 \times 64 \times 64$ grid. The solutions obtained by the WENO5-JS scheme and the various CRWENO5 schemes agree upstream of the shock, indicating that the grid resolution is sufficient. Downstream of the shock, the CRWENO5 schemes show a slight improvement over the WENO5-JS scheme. However, the various implementations of the weights have insignificant effects. Figure 25 compares the pre-shock ($x = -1$) and

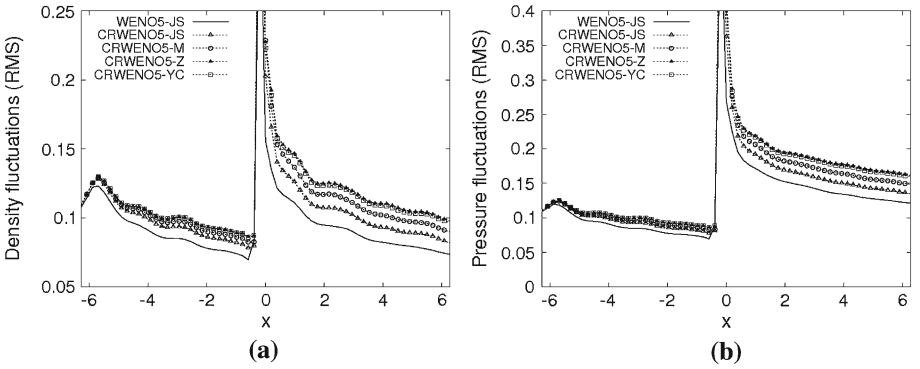

Fig. 23 Streamwise variation of density and pressure fluctuations on the $64 \times 32 \times 32$ grid. **a** Density, **b** pressure

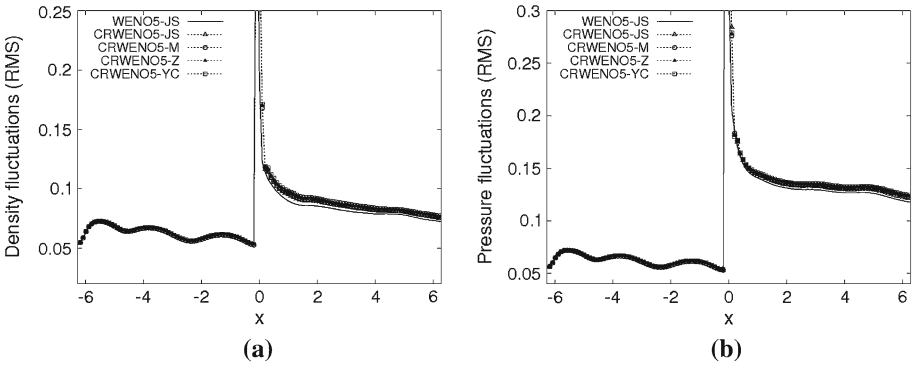

Fig. 24 Streamwise variation of density and pressure fluctuations on the $128 \times 64 \times 64$. **a** Density, **b** pressure grid

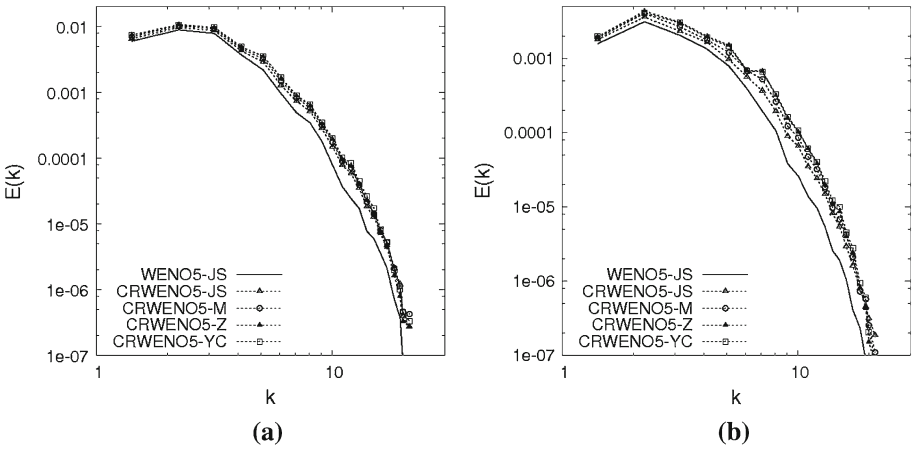

Fig. 25 Comparison of the energy spectra for solutions obtained on the $64 \times 32 \times 32$ grid. **a** Pre-shock ($x = -1$), **b** post-shock ($x = 6$)

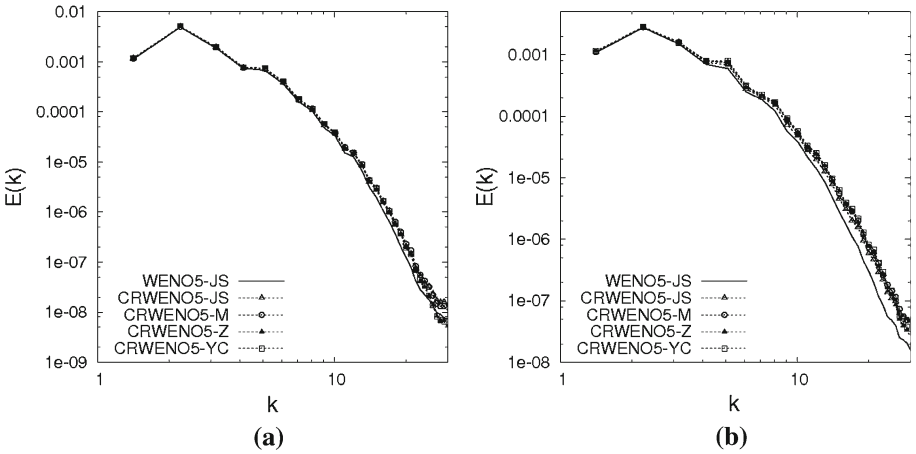

Fig. 26 Comparison of the energy spectra for solutions obtained on the $128 \times 64 \times 64$ grid. **a** Pre-shock ($x = -1$), **b** post-shock ($x = 6$)

post-shock ($x = 6$) energy spectra of the solutions obtained by the various schemes on the $64 \times 32 \times 32$ grid. The intermediate and smaller length scales are captured more accurately by the CRWENO5-JS scheme, compared to the WENO5 scheme, at both the pre- and post-shock locations. The alternative weights show only a marginal improvement of the resolution of these length scales upstream of the shock, while the improvements are significant downstream of the shock. This is due to the downstream fluctuations being of smaller length scales, which causes the solution to be more sensitive to the non-linear weights. Figure 26 shows the same for the solutions obtained on the $128 \times 64 \times 64$ grid. Similar solutions are observed upstream of the shock, with a good agreement between the solutions obtained by the WENO5-JS and the CRWENO5 schemes, indicating that the flow is well-resolved. The CRWENO5 schemes improve the resolution of the smaller length scales downstream of the shock, compared to

the WENO5-JS scheme, but the implementations of the non-linear weights do not have a significant effect on the solutions.

6 Conclusion

The performance of the fifth-order Compact-Reconstruction WENO scheme is demonstrated in this paper for flow problems characterized by a large range of length scales, as well as the presence of discontinuities. These include inviscid flow problems representative of compressible, turbulent flows and canonical turbulent flow problems. The CRWENO scheme uses a solution-dependent combination of lower-order accurate compact interpolation schemes at each interface, such that the resultant algorithm is high-order accurate for smooth solutions and non-oscillatory across discontinuities. The underlying linear scheme is a fifth-order compact interpolation scheme, and this results in superior numerical properties compared to the fifth-order WENO scheme based on a non-compact interpolation scheme.

The CRWENO scheme shows substantial improvements in the resolution of smaller length scales. This is observed for the inviscid interactions of an entropy wave and a vorticity wave with a normal shock, as well the DNS of decaying isotropic turbulence and the interaction of a turbulent flow with a normal shock. The high spectral resolution of the underlying linear scheme results in lower dissipation and phase errors for intermediate and high wavenumbers in the solution. In addition, this paper demonstrates the drawbacks of the original formulation of the non-linear weights in the context of turbulent flows. The various implementations of these weights, proposed in literature for the fifth-order WENO scheme, are studied in the context of the fifth-order CRWENO scheme. The original weights fail to distinguish between discontinuities and small length-scale waves, and this is alleviated to a large extent with the alternative formulations.

Thus, to conclude, the CRWENO schemes are a viable alternative for the DNS of compressible, turbulent flows. Compared to the hybrid compact-WENO schemes, it should be noted that the CRWENO schemes do not need to switch between two different families of interpolation methods to achieve non-oscillatory behavior. In addition, it does not revert to a non-compact scheme in the vicinity of discontinuities and thus, maintains a relatively high spectral resolution except at the discontinuity itself. This is a considerable advantage for flows dominated by a large number of discontinuities. The schemes presented in this paper are derived and implemented on uniform Cartesian grids. Application of these schemes to curvi-linear meshes will result in errors induced by the grid non-uniformity. Accurate simulation of turbulent flows on curvi-linear meshes require the derivation of these schemes for non-uniform grid spacing, and this is an area of future work.

Acknowledgments This research was supported by the U.S. Army's MAST CTA Center for Microsystem Mechanics with Mr. Chris Kroninger (ARL-VTD) as Technical Monitor.

References

1. Liu, X., Osher, S., Chan, T.: Weighted essentially non-oscillatory schemes. J. Comput. Phys. **115**, 200–212 (1994)
2. Jiang, G.-S., Shu, C.-W.: Efficient implementation of weighted ENO schemes. J. Comput. Phys. **126**, 202–228 (1996)
3. Shu, C.-W.: High order weighted essentially nonoscillatory schemes for convection dominated problems. SIAM Rev. **51**(1), 82–126 (2009)

4. Balsara, D.S., Shu, C.-W.: Monotonicity preserving weighted essentially non-oscillatory schemes with increasingly high order of accuracy. J. Comput. Phys. **160**, 405–452 (2000)
5. Lele, S.K.: Compact finite difference schemes with spectral-like resolution. J. Comput. Phys. **103**, 16–42 (1992)
6. Weinan, E., Liu, J.G.: Essentially compact schemes for unsteady viscous incompressible flows. J. Comput. Phys. **126**, 122–138 (1996)
7. Wilson, R.V., Demuren, A.Q., Carpenter, M.H.: High-order compact schemes for numerical simulation of incompressible flows. ICASE Report 98-13 (1998)
8. Lerat, A., Corre, C.: A residual-based compact scheme for the compressible Navier–Stokes equations. J. Comput. Phys. **170**, 642–657 (2001)
9. Ekaterinaris, J.A.: Implicit, high-resolution compact schemes for gas dynamics and aeroacoustics. J. Comput. Phys. **156**, 272–299 (1999)
10. Lee, C., Seo, Y.: A new compact spectral scheme for turbulence simulations. J. Comput. Phys. **183**, 438–469 (2002)
11. Nagarajan, S., Lele, S.K., Ferziger, J.H.: A robust high-order compact method for large eddy simulation. J. Comput. Phys. **191**, 392–419 (2003)
12. Cockburn, B., Shu, C.-W.: Nonlinearly stable compact schemes for shock calculation. SIAM J. Numer. Anal. **31**, 607–627 (1994)
13. Yee, H.C.: Explicit and implicit multidimensional compact high-resolution shock-capturing methods: formulation. J. Comput. Phys. **131**, 216–232 (1997)
14. Adams, N.A., Shariff, K.: A high-resolution hybrid compact-ENO scheme for shock-turbulence interaction problems. J. Comput. Phys. **127**, 27–51 (1996)
15. Pirozzoli, S.: Conservative hybrid compact-WENO schemes for shock-turbulence interaction. J. Comput. Phys. **178**, 81–117 (2002)
16. Ren, Y.-X., Liu, M., Zhang, H.: A characteristic-wise hybrid compact-WENO scheme for solving hyperbolic conservation laws. J. Comput. Phys. **192**, 365–386 (2003)
17. Deng, X., Zhang, H.: Developing high order weighted compact nonlinear schemes. J. Comput. Phys. **165**, 22–44 (2000)
18. Zhang, S., Jiang, S., Shu, C.-W.: Development of nonlinear weighted compact schemes with increasingly higher order accuracy. J. Comput. Phys. **227**, 7294–7321 (2008)
19. Wang, Z., Huang, G.P.: An essentially nonoscillatory high order Padé-type (ENO-Padé) scheme. J. Comput. Phys. **177**, 37–58 (2002)
20. Ghosh, D., Baeder, J.D.: Compact reconstruction schemes with weighted ENO limiting for hyperbolic conservation laws. SIAM J. Sci. Comput. **34**(3), A1678–A1706 (2012)
21. Ghosh, D.: Compact-Reconstruction Weighted Essentially Non-Oscillatory Schemes for Hyperbolic Conservation Laws. Ph.D. thesis, University of Maryland, College Park, (2013)
22. Ghosh, D., Medida, S., Baeder, J.D.: Compact-reconstruction weighted essentially non-oscillatory schemes for unsteady Euler/Navier-Stokes equations. In: AIAA Paper 2012-2832, 42nd AIAA Fluid Dynamics Conference and Exhibit, New Orleans, LA 25–28 June, 2012
23. Henrick, A.K., Aslam, T.D., Powers, J.M.: Mapped weighted essentially non-oscillatory schemes: achieving optimal order near critical points. J. Comput. Phys. **207**, 542–567 (2005)
24. Borges, R., Carmona, M., Costa, B., Don, W.S.: An improved weighted essentially non-oscillatory scheme for hyperbolic conservation laws. J. Comput. Phys. **227**, 3191–3211 (2008)
25. Yamaleev, N.K., Carpenter, M.H.: A systematic methodology for constructing high-order energy stable WENO schemes. J. Comput. Phys. **228**, 4248–4272 (2009)
26. Pirozzoli, S.: On the spectral properties of shock-capturing schemes. J. Comput. Phys. **219**, 489–497 (2006)
27. Fauconnier, D., Dick, E.: On the spectral and conservation properties of nonlinear discretization operators. J. Comput. Phys. **230**, 4488–4518 (2011)
28. Shu, C.-W., Osher, S.: Efficient implementation of essentially non-oscillatory shock capturing schemes. J. Comput. Phys. **77**, 439–471 (1988)
29. Shu, C.-W., Osher, S.: Efficient implementation of essentially non-oscillatory shock capturing schemes, II. J. Comput. Phys. **83**, 32–78 (1989)
30. Martín, M.P., Taylor, E.M., Wu, M., Weirs, V.G.: A bandwidth-optimized WENO Scheme for the direct numerical simulation of compressible turbulence. J. Comput. Phys. **220**, 270–289 (2006)
31. Taylor, E.M., Martín, M.P.: Stencil adaptation properties of a WENO scheme in direct numerical simulations of compressible turbulence. J. Sci. Comput. **30**(3), 533–554 (2007)
32. Tam, C.K.W., Webb, J.C.: Dispersion-relation-preserving finite difference schemes for computational acoustics. J. Comput. Phys. **107**, 262–281 (1993)

33. Rogallo, R.S.: Numerical experiments in homogenous turbulence. NASA Technical Memorandum 81315 (1981)
34. Mansour, N.N., Wray, A.A.: Decay of isotropic turbulence at low Reynolds number. Phys. Fluids **6**(2), 808–814 (1994)
35. Lee, S., Lele, S.K., Moin, P.: Direct numerical simulation of isotropic turbulence interacting with a weak shock wave. J. Fluid Mech. **251**, 533–562 (1993)
36. Lee, S., Lele, S.K., Moin, P.: Interaction of isotropic turbulence with shock waves: effect of shock strength. J. Fluid Mech. **340**, 225–247 (1997)
37. Mahesh, K., Lele, S.K., Moin, P.: The influence of entropy fluctuations on the interaction of turbulence with a shock wave. J. Fluid Mech. **334**, 353–379 (1997)
38. Larsson, J., Lele, S.K.: Direct numerical simulation of canonical shock/turbulence interaction. Phys. Fluids **21**(12), (2009) paper 126101
39. Colonius, T., Lele, S.K., Moin, P.: Boundary conditions for direct computation of aerodynamic sound. AIAA J. **31**, 1574–1582 (1993)
40. Freund, J.B.: Proposed inflow/outflowboundary condition for direct computation of aerodynamic sound. AIAA J. **35**, 740–742 (1997)
41. Lee, S., Moin, P., Lele, S.K.: Interaction of isotropic turbulence with a shock wave. Report TF-52, Thermosciences Division, Department of Mechanical Engineering, Stanford University (1992)
42. Mahesh, K., Moin, P., Lele, S.K.: The interaction of a shock wave with a turbulent shear flow. Report TF-69, Thermosciences Division, Department of Mechanical Engineering, Stanford University (1996)